Journal of Radioanalytical and Nuclear Chemistry (2018) 316:963–970
https://doi.org/10.1007/s10967-018-5751-2

Improved Eu(III) immobilization by *Cladosporium sphaerospermum* induced by low-temperature plasma

Jun Liang[1] · Lvmu Li[1] · Wencheng Song[2,3]

Received: 20 September 2017 / Published online: 5 March 2018

Abstract
To increase the bioaccumulation of Eu(III), low temperature plasma as a method of mutagenesis was introduced to mutate *Cladosporium sphaerospermum* (*C. sphaerospermum*). Mycelia doses, pH, and ionic strength obviously affected the Eu(III) immobilization on mycelia. The maximum immobilization capacities of Eu(III) on mutated *C. sphaerospermum* was 278.8 mg/g at pH 6.5, which was approximately three times than that of raw *C. sphaerospermum*. Before and after Eu(III) loaded mycelia were analyzed by XPS and FTIR, and intracellular structures of mycelia changed obviously under Eu(III) stress by TEM analysis. The results suggested that low temperature plasma could be utilized as a valuable treatment technology to improve fungi for the removal and immobilization of radionuclides in the environment.

Keywords Immobilization · *Cladosporium sphaerospermum* · Eu(III) · Low temperature plasma

Introduction

Long-lived radionuclides posed serious threats to biological systems and human health due to its potential toxic and carcinogenic effects [1]. Europium (Eu(III)), one of the fission products of uranium, was often used as a chemical analogue for trivalent lanthanides/actinides in removal studies because of their comparable physicochemical properties and similar environmental behaviors [2–4]. Therefore, developing cost-effective and environment-friendly materials to remove Eu(III) from environments are of particular importance. There are lots of materials for Eu(III) removal, such as carbon materials [5–9], metal oxides [10–12] and clay minerals [13–15]. However, removal of radionuclides or heavy metal by microorganisms has been demonstrated to be more environmentally friendly and cheaper than chemical and physical materials, especially in the aspect of stimulating indigenous microbial communities [16]. Among microorganisms, fungi have advantages over bacteria for the bioremediation of contaminated sites owing to its mycelia network, biomass and longer life-cycle [17]. Moreover, radionuclides or metals tolerant fungi can compete with the native bacteria in hostile situations and have developed different strategies to protect themselves from oxidative stress caused by radionuclides or metals [18–20]. However, as far as we know studies about Eu(III) immobilization on fungi were still little [16].

Low temperature plasma (LTP) generated free electrons and ions, radicals and a variety of radiation ranging from UV via visible to infrared [21]. Research showed that LTP treatment could lead to intensively microbial DNA change, suggesting that LTP was expected to be used for microbial mutagenesis [22]. Therefore, LTP was successfully applied in many microbial mutagenesis [23–26].

LTP as a method of mutagenesis was introduced to mutate *Cladosporium sphaerospermum* (*C. sphaerospermum*) in order to improve $^{152+154}$Eu(III) immobilization. Eu(III) immobilization on mutated *C. sphaerospermum*

✉ Lvmu Li
lilvmu@126.com

✉ Wencheng Song
wencsong@hotmail.com

[1] School of Life Science, Anhui Agricultural University, Hefei 230036, People's Republic of China

[2] Anhui Province Key Laboratory of Medical Physics and Technology, Center of Medical Physics and Technology, Hefei Institutes of Physical Science, Chinese Academy of Sciences, Hefei 230031, People's Republic of China

[3] Hefei Cancer Hospital, Chinese Academy of Sciences, Hefei 230031, People's Republic of China

was studied in different environmental conditions, and characterization of Eu(III) immobilization on mycelia was investigated by X-ray photoelectron spectroscopy (XPS), Fourier transform infrared spectroscopy (FTIR), and transmission electron microscopy (TEM). This study will better understand the Eu(III) immobilization mechanism on fungi and improve the bioremediation strategies of Eu(III) pollution.

Materials and methods

Cultivation of resistant fungus

Resistant fungus used in this study was isolated from radionuclide-contaminated soils, and the method of isolation and identification had been shown in previous study [16]. Cultivation of the fungus was carried out in 250 ml Erlenmeyer flasks with 100 ml potato dextrose agar (PDA) medium on a rotary shaker at 200 rpm and 28 °C. After 3 days' cultivation, mycelia were harvested by centrifugation, washed three times in deionized water and stored at 4 °C for batch experiments. Besides, mycelia were trapped under glass using laetophcnol cotton lalue stain before being examined, and observed under an Olympus IX71 inverted fluorescence microscope (Olympus, Tokyo, Japan). All images were captured using a TH4-200 photo system (Olympus, Tokyo, Japan) at ×200 magnification.

Characterization of fungal mycelia

Fungus was incubated in PDA medium containing 0 or 200 mg/l Eu(III) at 28 °C and 200 rpm for 3 days. The samples for TEM were fixed in 5% glutaraldehyde for 3 h, then post-fixed in 1.0% osmium tetraoxide for 2 h and dehydrated in a graded ethanol series (50–100%) as previously described by El-Sayed [27]. The blocks were sectioned, stained and observed using a TEM with an energy dispersive X-ray analysis (EDS) (Hitachi HT-7700, Japan). The method of XPS (Thermo ESCALAB 250, USA), and FTIR (Perkin Elmer 100, USA) referred to related literature [16].

Eu(III) immobilization by mycelia

Immobilization of Eu(III) by mycelia was studied under ambient conditions. The different concentrations of mycelia suspensions, Eu(III) and NaCl solution were added into Erlenmeyer flasks, and pH of the solution was regulated to 6.5. After immobilization equilibrium, the solution was centrifuged at 8000 rpm for 10 min, and $^{152+154}$Eu(III) concentration was analyzed by Liquid Scintillation counting (Packard 3100 TR/AB Liquid Scintillation analyzer, Perkin-Elmer) with the scintillation cocktail (ULTIMA GOLD ABTM, Packard). The immobilization percentage and amounts of Eu(III) immobilization capacity (Q, mg/g) were described as Eqs. (1) and (2):

$$\text{Immobilization } \% = (C_0 - C_e) \times 100\,\%/C_0 \quad (1)$$

$$Q_t = (C_0 - C_e) \times V/m \quad (2)$$

where C_0 and C_e (mg/l) were initial and equilibrium concentrations, respectively. V and m were volume of suspension and the mass of mycelia, respectively. All tests were conducted in triplicate.

Results and discussion

Isolate mutagenesis experiments

The LTP plasma was schematically illustrated in Fig. 1a, which was described in previous studies [28–30]. The reactor chamber has three poles, one air inlet and one air outlet. In the experiment, we used helium (99.99% pure) gas as work gas which flow rates was 80 l/h and injected 3 min before the experiment to expel air as much as possible from reactor chamber. Spores were collected, and diluted spore samples were mutated by LTP for 6 min. LTP was generated by voltage of 30 V and power of 42 W. Then, mutated spores were inoculated onto PDA petriplates containing Eu(III). Then, the best mutant isolate was selected from morphology and cultured for immobilization experiments.

Identification of the isolate

The length of ITS sequence of the isolate was approximately 526 bp. It showed 99% similarity with *C. sphaerospermum* in GenBank (KJ191437.1 and HG530663.1). Combining with external morphological features as shown in Fig. 1b, the isolate was identified as *C. sphaerospermum*.

Effect of time

The amount of Eu(III) immobilization on *C. sphaerospermum* increased linearly with time during the first 24 h, and then remained almost constant within 84 h (Fig. 2a). The initial observed immobilization rate of Eu(III) on mycelia was very fast, whereas it became slow in the second phase, which was in accordance with the previously Eu(III) immobilization study [12]. That was because at initial stages of the immobilization, the higher concentration of Eu(III) provided the driving force to facilitate Eu(III) diffusion from solution to the active sites of mycelia. As the

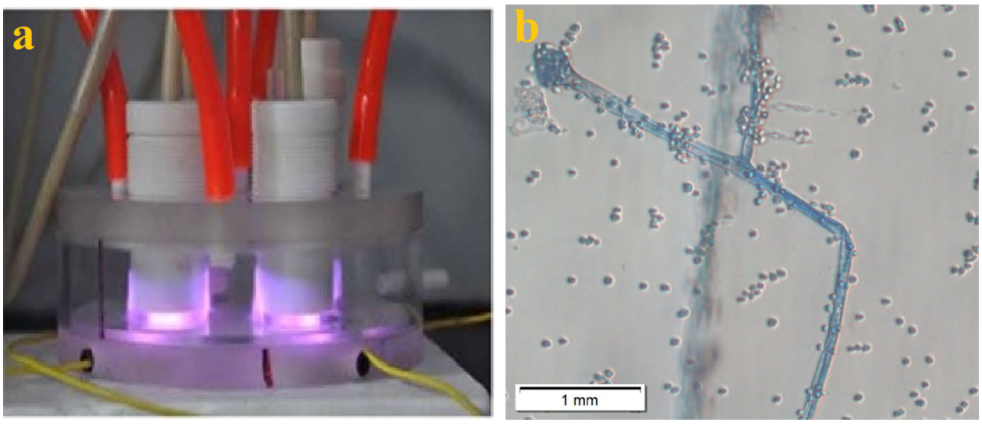

Fig. 1 The schematic of the plasma system and photograph of the reactor chamber (**a**), light microscopes images of *C. sphaerospermum* (**b**)

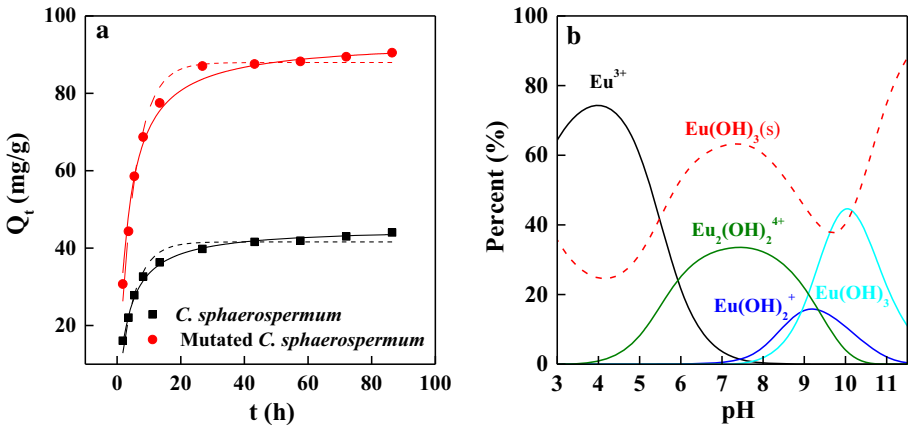

Fig. 2 Effect of contact time on Eu(III) immobilization (**a**), $T = 295$ K, m/V = 0.4 g/l, $C_{[Eu(III)]initial} = 40$ mg/l. Relative distribution of Eu(III) species as a function of pH based on the equilibrium constants, $pCO_2 = 3.2 \times 10^{-4}$ atm (**b**)

process continued, the decrease of Eu(III) concentration and the active sites of mycelia resulted in the decrease in Eu(III) immobilization [31]. Data points were fitted better with the pseudo-second-order kinetic model as compared to pseudo-first-order kinetic model, and kinetic parameters and equations from both models were listed in Table 1. The results of kinetics indicated that *C. sphaerospermum* possessed high immobilization efficiency for Eu(III).

Effect of pH

Several factors caused changes in Eu(III) accumulation as pH levels were modified. For example, Eu(III) species changed with the increase of pH (Fig. 2b). Besides, changes in pH could produce modifications in the surface net charge of mycelia. The immobilization Eu(III) on *C. sphaerospermum* and mutated *C. sphaerospermum* increased obviously as pH increased between 2.0 and 7.0, and maintained high level at pH > 7.0 (Fig. 3a). About 80% Eu(III) accumulated on mutated *C. sphaerospermum* at pH 6.5, which was about 30% more than that of *C. sphaerospermum*. The electrostatic interaction between mutated *C. sphaerospermum* and Eu(III) resulted in lower immobilization at pH < 7.0. Higher immobilization of Eu(III) at pH > 7.0 could belong to electrostatic attraction

Table 1 Parameters for immobilization kinetic data using different models

Models	Pseudo-first-order			Pseudo-second-order		
	Q(mg/g)	K (1/h)	R^2	Q(mg/g)	K' (g/(mg h))	R^2
Equations	$Q_t = Q\ (1 - \exp(-K))$			$t/Q_t = 1/K'Q^2 + t/Q$		
C. sphaerospermum	41.607	0.27675	0.965	45.3195	0.01134	0.998
Mutated *C. sphaerospermum*	86.66	0.298	0.986	92.665	0.0108	0.999

C_0 and C_e (mg/l) were initial and equilibrium concentrations, respectively. V and m were volume of suspension and biomass of mycelia, respectively

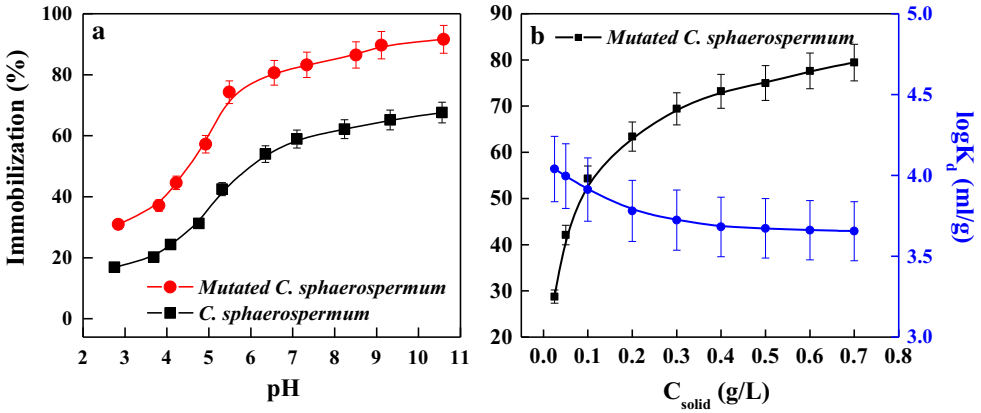

Fig. 3 Effect of pH on Eu(III) immobilization to *C. sphaerospermum* and mutated *C. sphaerospermum* (**a**), the effect of mycelia doses on Eu(III) immobilization to mutated *C. sphaerospermum* (**b**), $T = 295$ K, $C_{[Eu(III)]initial} = 40$ mg/l

between Eu(III) and mycelia as well as the precipitates of $Eu(OH)_3$ [32].

Effect of mycelia doses

The influence of mycelia doses on capacity of mutated *C. sphaerospermum* immobilization Eu(III) from aqueous solution was studied by using different fungal doses in the range of 0.05–0.7 g/l (Fig. 3b). The immobilization of Eu(III) rapidly rised with the increase of mutated *C. sphaerospermum* doses. It's because more available sites for immobilization as well as greater surface area for immobilization ascended with the increase of mutated *C. sphaerospermum* doses. Oppositely, K_d reduced with the increase of mutated *C. sphaerospermum* doses, because the aggregation of fungal mycelia and competition among fungal mycelia reduced effective enrichment sites on mutated *C. sphaerospermum* [33].

Effect of ionic strength

The immobilization of Eu(III) on mycelia as a function of NaCl strength was shown in Fig. 4a. Eu(III) immobilization onto *C. sphaerospermum* and mutated *C. sphaerospermum* percent decreased with the increase of NaCl strength. The immobilization percent of Eu(III) on *C. sphaerospermum* and mutated *C. sphaerospermum* decreased 20 and 11% from 0.01 to 0.05 mol/l NaCl, respectively. That might be ascribed to the decrease of competing NaCl strength led to the formation of electrical double layer complexes, which favored the accumulation of Eu(III) on mycelia. The phenomenon was indicative of an ion exchange mechanism. On the other hand, NaCl strength of solution influenced the activity coefficient of Eu(III), which limited their transfer to mycelia [34].

Immobilization isotherms

Eu(III) immobilization isotherms of *C. sphaerospermum* and mutated *C. sphaerospermum* were illustrated in Fig. 4b. At pH 6.5 and 295 K, the increase of Eu(III) immobilization on *C. sphaerospermum* and mutated *C. sphaerospermum* was observed distinctly with the increase of Eu(III) doses. Two isotherms models (Langmuir and Freundlich models) were used to simulate the experimental data. From Fig. 4b and Table 2, Langmuir model simulated the experimental data better than Freundlich, and the maximum immobilization capacities ($C_{s\ max}$) of Eu(III) on mutated *C. sphaerospermum* was 278.8 mg/g at pH 6.5, which was approximately three times than that of raw *C.*

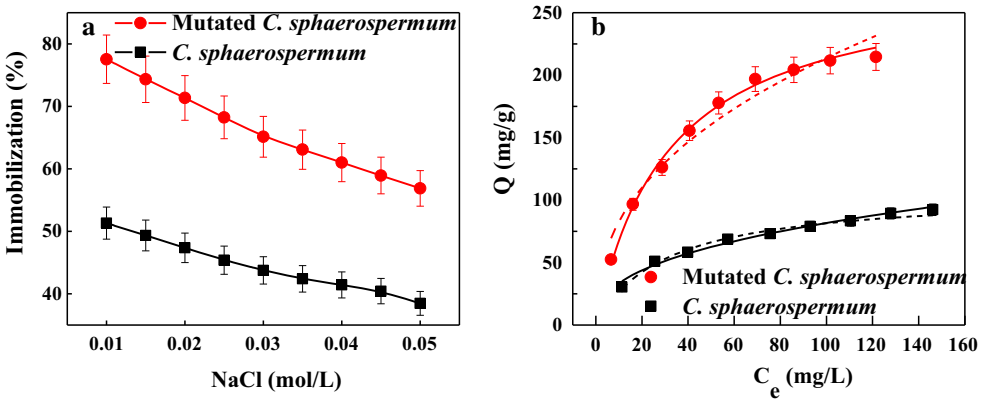

Fig. 4 Effect of ionic strength on Eu(III) immobilization by *C. sphaerospermum* and mutated *C. sphaerospermum* (**a**), the isotherms of Eu(III) on *C. sphaerospermum* and mutated *C. sphaerospermum*, the solid line stands for Langmuir model and the dash line stands for Freundlich model (**b**), $T = 295$ K, m/V = 0.4 g/l

Table 2 Parameters for the Langmuir and Freundlich isotherm models

Biosorbent	Langmuir model			Freundlich model		
Equations	$C_{s\ max}$ (mg/g)	b (l/mg) $Q = b \times Q_{max} \times C_e/(1 + b \times C_e)$	R^2	K_F ($mg^{1-n}\ l^n/g$) $Q = K_F \times C_e^n$	n	R^2
C. sphaerospermum	93.07	0.0301	0.998	14.352	0.3839	0.986
Mutated *C. sphaerospermum*	278.8	0.0316	0.998	31.334	0.4178	0.961

$C_{s\ max}$ was theoretical maximum immobilization capacity per unit weight of mycelia. K_F and b were immobilization constants of Freundlich and Langmuir, respectively

sphaerospermum. Besides, $C_{s\ max}$ of mutated *C. sphaerospermum* was also higher than Eu(III) onto other biomaterials, such as *Mycobacterium smegmatis* (19.15 mg/g at pH 5.0), *Pseudomonas aeruginosa* (44.1 mg/g at pH 5.0 and 293 K), and *Sargassum* sp. [35–37]. These results indicated that mutated *C. sphaerospermum* was a feasible and efficacious material to control Eu(III) pollution in the environment.

XPS and FTIR analysis

XPS spectra demonstrated the sensitivity for identifying elements on mycelia. Therefore, the XPS technique was applied to investigate immobilization mechanism. The XPS spectra of Eu(III) immobilized on mutated *C. sphaerospermum* was shown in Fig. 5a. After immobilization, peaks at 1134.6 and 1164.4 eV were attributed to Eu $3d_{5/2}$ and Eu $3d_{3/2}$, respectively, which demonstrated the high absorbability of mutated *C. sphaerospermum* for Eu(III). Compared to mutated *C. sphaerospermum*, C, N, and O percentage of mutated *C. sphaerospermum*- Eu(III) correspondingly declined from XPS analysis (Table 3), which indicated Eu(III) immobilization on mutated *C. sphaerospermum* was partially related to groups contained O and N atoms on the surface of mycelia [38–40].

The FT-IR spectra of unloaded and Eu(III) loaded mutated *C. sphaerospermum* were presented in Fig. 5b. It showed some distinct peaks at 1034 cm^{-1} (> S=O), 1246 cm^{-1} (the amide III band, C–N stretch), 1332 cm^{-1} (C–O stretches), 1442 cm^{-1} (stretching of COO–), 1560 cm^{-1} (the amide II band, C–N stretching and N–H bending vibration), 1656 cm^{-1} (the amide I band, C=O stretching), 1748 cm^{-1} (> C=O stretching), 2926 cm^{-1} (–CH stretching vibrations), and band at 3200–3500 cm^{-1} (O–H and N–H stretching vibrations) [41, 42]. After Eu(III) immobilization, peaks of C–N stretching and carboxyl groups (C–O) shifted, which showed it contributed to the complexation between Eu(III) and mutated *C. sphaerospermum* [43]. XPS and FTIR analysis revealed amino, hydroxyl, and carboxyl groups were responsible for Eu(III) immobilization onto mutated *C. sphaerospermum*.

Changes of subcellular structure under Eu(III) stress

TEM was used to investigate the changes of subcellular structure of mutated *C. sphaerospermum* before and after Eu(III) exposure in the same nutritional state. No obvious change in extracellular structure of mutated *C. sphaerospermum* was observed before and after Eu(III) exposure (Fig. 6). There were some electron-dense bodies in the

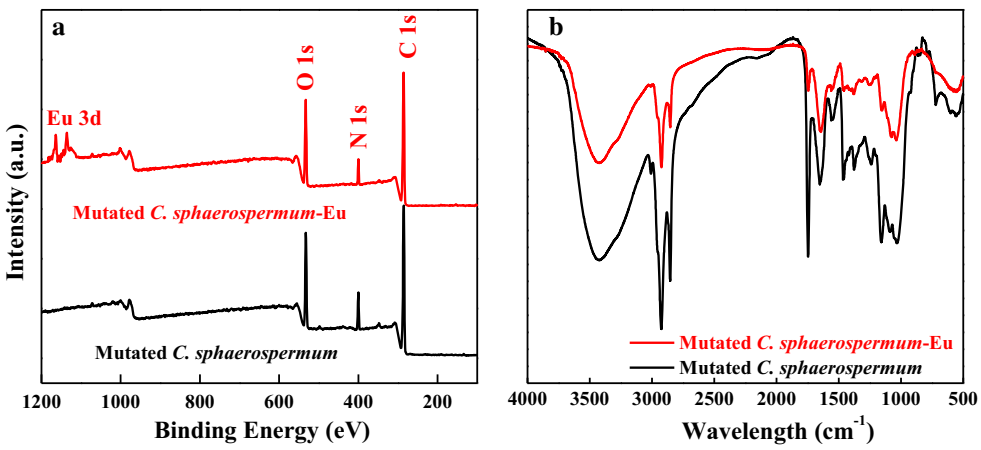

Fig. 5 XPS survey scan and high resolution spectra of mutated *C. sphaerospermum* and mutated *C. sphaerospermum*-Eu, total survey scans spectr (**a**), FTIR spectra of mutated *C. sphaerospermum* and mutated *C. sphaerospermum*-Eu (**b**). pH 6.5, m/V = 0.4 g/l, $C_{[EU(III)]initial}$ = 40 mg/l

Table 3 Atomic percentage of Mutated *C. sphaerospermum* and Mutated *C. sphaerospermum*- Eu(III) from the XPS data

Element	Mutated *C. sphaerospermum*		Mutated *C. sphaerospermum*-Eu	
	BE (eV)	%	BE (eV)	%
C 1*s*	286.04	72.65	286.45	70.97
O 1*s*	532.4	20.94	532.41	19.51
N 1*s*	399.73	4.88	399.99	4.49
Eu 3*d*				3.95

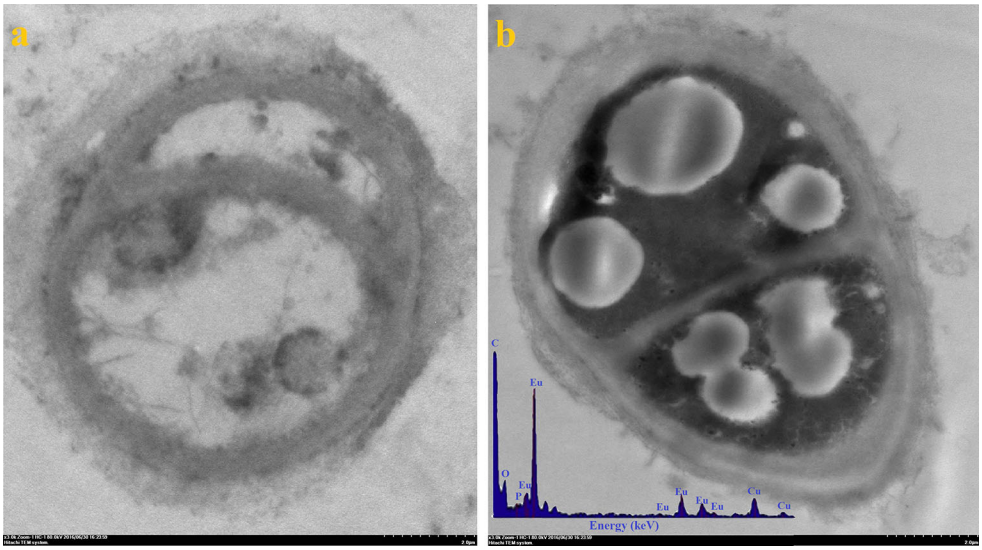

Fig. 6 TEM images of Eu(III) loaded *C. sphaerospermum* (**a**, **b**) at 0 and 200 mg/l Eu(III) for 3 days, respectively

cells of mutated *C. sphaerospermum* after exposure Eu(III). The EDS spectra derived from electron-dense bodies indicated that they were consisted of carbon, oxygen, phosphorus, europium and copper. The copper band was from the grid used to support sections (Fig. 6b). The detoxification of Eu(III) by mutated *C. sphaerospermum* might be mediated through thiol compounds, which bound intracellular free Eu(III) in order to reduce damage to the metabolic process [44]. These changes might be part of the adaptation mechanism of fungi to metal toxicity according to previous results. The intracellular electron-dense area was revealed by TEM, indicating chromate penetration into the cell of *Aspergillus niger* [45]. TEM and EDS of *Pseudomonad* (CRB5) also demonstrated U(VI) appeared in the cell [46]. Besides, the analysis of TEM and EELS indicated that excessive amounts of Cu(II) induced sub-cellular changes of *Allium sativum* L. [47].

Conclusions

In this study, *C. sphaerospermum* was mutated by LTP to enhance Eu(III) immobilization. The mutated *C. sphaerospermum* presented higher adsorbability for Eu(III) immobilization investigated by batch experiments, and Langmuir model simulated the experimental data better than Freundlich model. The results of XPS and FTIR showed that carboxyl, hydroxyl and amino groups on mycelia favored Eu(III) immobilization on mutated *C. sphaerospermum*, and intracellular structures of mycelia changed obviously under Eu(III) stress by TEM analysis. These results were crucial for further understanding the transportation and accumulation of radionuclides on fungi in environmental cleanup.

Acknowledgements This research was supported by National Natural Science Foundation of China (21607156) and China Postdoctoral Science Foundation funded project (2015M581047).

References

1. Sheng GD, Yang ST, Li YM, Gao X, Huang YY, Hu J, Wang XK (2014) Retention mechanisms and microstructure of Eu(III) on manganese dioxide studied by batch and high resolution exafs technique. Radiochim Acta 102:155–167
2. Fan QH, Tan XL, Li JX, Wang XK, Wu WS, Montavon G (2009) Sorption of Eu(III) on attapulgite studied by batch, XPS, and EXAFS techniques. Environ Sci Technol 43:5776–5782
3. Wang XX, Yang SB, Shi WQ, Li JX, Hayat T, Wang XK (2015) Different interaction mechanisms of Eu(III) and ^{243}Am (III) with

carbon nanotubes studied by batch, spectroscopy technique and theoretical calculation. Environ Sci Technol 49:11721–11728
4. Wang XX, Yu SJ, Chen ZS, Song WC, Chen YT, Hayat T, Alsaedi A, Guo W, Hu J, Wang XK (2015) Complexation of radionuclide $^{152+154}$Eu (III) with alumina-bound fulvic acid studied by batch and time-resolved laser fluorescence spectroscopy. Sci China Chem 60:107–114
5. Sun YB, Wu ZY, Wang XX, Ding CC, Cheng WC, Yu SH, Wang XK (2016) Macroscopic and microscopic investigation of U(VI) and Eu(III) adsorption on carbonaceous nanofibers. Environ Sci Technol 50:4459–4467
6. Chen CL, Wang XK, Nagatsu M (2009) Europium adsorption on multiwall carbon nanotube/iron oxide magnetic composite in the presence of polyacrylic acid. Environ Sci Technol 43:2362–2367
7. Xie Y, Helvenston EM, Shuller-Nickles LC, Powell BA (2016) Surface complexation modeling of Eu(III) and U (VI) interactions with graphene oxide. Environ Sci Technol 50:1821–1827
8. Sun YB, Lu SH, Wang XX, Xu C, Li JX, Chen CL, Chen J, Hayat T, Alsaedi A, Alharbi NS, Wang XK (2017) Plasma-facilitated synthesis of amidoxime/carbon nanofiber hybrids for effective enrichment of 238 U(VI) and 241 Am(III). Environ Sci Technol 51:12274–12282
9. Yu SJ, Wang XX, Yang ST, Sheng GD, Alsaedi A, Hayat T, Wang XK (2017) Interaction of radionuclides with natural and manmade materials using XAFS technique. Sci China Chem 60:170–187
10. Bouby M, Lutzenkirchen J, Dardenne K, Preocanin T, Denecke MA, Klenze R, Geckeis H (2010) Sorption of Eu(III) onto titanium dioxide: measurements and modeling. J Colloid Interface Sci 350:551–561
11. Konstantinou M, Pashalidis I (2008) Competitive sorption of Cu(II), Eu(III) and U(VI) ions on TiO_2 in aqueous solutions—a potentiometric study. Coll Surf A 324:217–221
12. Wang XX, Yu SJ, Chen ZS, Zhao YS, Jin J, Wang XK (2017) Microstructures and speciation of radionuclides in natural environment studied by advanced spectroscopy and theoretical calculation. Sci China Chem 60:1149–1152
13. Galunin E, Alba MD, Santos MJ, Abrão T, Vidal M (2010) Lanthanide sorption on smectitic clays in presence of cement leachates. Geochim Cosmochim Acta 74:862–875
14. Schnurr A, Marsac R, Rabung T, Lützenkirchen J, Geckeis H (2015) Sorption of Cm(III) and Eu(III) onto clay minerals under saline conditions: batch adsorption, laser-fluorescence spectroscopy and modeling. Geochim Cosmochim Acta 151:192–202
15. Dolatyari L, Yaftian MR, Rostamnia S (2016) Adsorption characteristics of Eu(III) and Th(IV) ions onto modified mesoporous silica SBA-15 materials. J Taiwan Inst Chem Eng 60:174–184
16. Song WC, Liang J, Wen T, Wang XX, Hu J, Hayat T, Alsaedi A, Wang XK (2016) Accumulation of Co(II) and Eu(III) by the mycelia of *Aspergillus niger* isolated from radionuclide-contaminated soils. Chem Eng J 304:186–193
17. Singh M, Srivastava PK, Verma PC, Kharwar RN, Singh N, Tripathi RD (2015) Soil fungi for mycoremediation of arsenic pollution in agriculture soils. J Appl Microbiol 119:1278–1290
18. Purchase D, Scholes LNL, Shutes Revitt DM (2009) Effects of temperature on metal tolerance and the accumulation of Zn and Pb by metal-tolerant fungi isolated from urban runoff treatment wetlands. J Appl Microbiol 106:1163–1174
19. Sun J, Zou X, Ning Z, Sun M, Peng J, Xiao T (2012) Culturable microbial groups and thallium-tolerant fungi in soils with high thallium contamination. Sci Total Environ 441:258–264
20. Wu Y, Wen Y, Zhou J, Dai Q, Wu Y (2012) The characteristics of waste *Saccharomyces cerevisiae* biosorption of arsenic(III). Environ Sci Pollut Res 19:3371–3379
21. Laroussi M, Richardson JP, Dobbs FC (2002) Effects of nonequilibrium atmospheric pressure plasmas on the heterotrophic pathways of bacteria and on their cell morphology. Appl Phys Lett 81:772–774
22. Zhang X, Zhang XF, Li HP, Wang LY, Zhang C, Xing XH, Bao CY (2014) Atmospheric and room temperature plasma (ARTP) as a new powerful mutagenesis tool. Appl Microbiol Biotechnol 98:5387–5396
23. Chen HX, Xiu ZL, Bai FW (2014) Improved ethanol production from xylose by *Candida shehatae* induced by dielectric barrier discharge air plasma. Plasma Sci Technol 16:602–607
24. Dong XY, Xiu ZL, Li S, Hou YM, Zhang DJ, Ren CS (2010) Dielectric barrier discharge plasma as a novel approach for improving 1,3-propanediol production in *Klebsiella pneumoniae*. Biotechnol Lett 32:1245–1250
25. Wang LY, Huang ZL, Li G, Zhao HX, Xing XH, Sun WT (2010) Novel mutation breeding method for *Streptomyces avermitilis*, using an atmospheric pressure glow discharge plasma. J Appl Microbiol 108:851–858
26. Qi F, Kitahara Y, Wang Z, Zhao X, Du W, Liu D (2014) Novel mutant strains of *Rhodosporidium toruloides* by plasma mutagenesis approach and their tolerance for inhibitors in lignocellulosic hydrolyzate. J Chem Technol Biotechnol 89:735–742
27. El-Sayed MT (2015) An investigation on tolerance and biosorption potential of Aspergillus awamori ZU JQ 965830.1 to Cd(II). Ann Microbiol 65:69–83
28. Song WC, Wang XX, Tao W, Wang H, Hayat T, Wang XK (2016) Enhanced accumulation of U(VI) by *Aspergillus oryzae* mutant generated by dielectric barrier discharge air plasma. J Radioanal Nucl Chem 310:1353–1360
29. Ma J, Zhang H, Cheng C, Shen J, Bao L, Han W (2016) Contribution of hydrogen peroxide to non-thermal atmospheric pressure plasma induced a549 lung cancer cell damage. Plasma Proces Polym 9999:1–12
30. Song WC, Wang EJ, Gao Y, Wu JB, Rao SH, Wang HZ, Bao LZ (2017) Low temperature plasma induced apoptosis in CNE-2Z cells through endoplasmic reticulum stress and mitochondrial dysfunction pathways. Plasma Proces Polym. https://doi.org/10.1002/ppap.201600249
31. Prasad KS, Ramanathan AL, Paul J, Subramanian V, Prasad R (2013) Biosorption of arsenite (As + 3) and arsenate (As + 5) from aqueous solution by *Arthrobacter sp.* biomass. Environ Technol 34:2701–2708
32. Yuzer H, Kara M, Sabah E, Celik MS (2008) Some experiments on the precipitation of suspensoid protein by various ions and some suggestions as to its cause. J Hazard Mater 151:33–37
33. Strawn DG, Sparks DL (1999) The use of XAFS to distinguish between inner- and outer-sphere lead adsorption complexes on montmorillonite. J Colloid Interf Sci 216:257–269
34. Ding CC, Feng S, Cheng W, Zhang J, Li X, Liao J, Liu N (2014) Biosorption behavior and mechanism of thorium on *Streptomyces sporoverrucosus* dwc-3. J Radioanal Nucl Chem 301:237–245
35. Texier AC, Andres Y, Cloirec PL (1997) Selective biosorption of lanthanide (La, Eu) ions by *Mycobacterium smegmatis*. Environ Technol 18:835–841
36. Texier AC, Andres Y, Cloirec PL (1999) Selective biosorption of lanthanide (La, Eu, Yb) ions by *Pseudomonas aeruginosa*. Environ Sci Technol 33:489–495
37. Oliveira RC, Hammer P, Guibal E, Taulemesse JM, Garcia O (2014) Characterization of metal–biomass interactions in the lanthanum(III) biosorption on *Sargassum* sp. using SEM/EDX, FTIR, and XPS: preliminary studies. Chem Eng J 239:381–391
38. Song WC, Wang XX, Wang Q, Shao DD, Wang XK (2015) Plasma-induced grafting of polyacrylamide on graphene oxide nanosheets for simultaneous removal of radionuclides. Phys Chem Chem Phys 17:398–406
39. Yuan SJ, Sun M, Sheng GP, Li Y, Li WW, Yao RS, Yu HQ (2010) Identification of key constituents and structure of the

extracellular polymeric substances excreted by Bacillus megaterium TF10 for their flocculation capacity. Environ Sci Technol 45:1152–1157
40. Tan XL, Fan QH, Wang XK, Grambow B (2009) Eu(III) sorption to TiO_2 (anatase and rutile): batch, XPS, and EXAFS studies. Environ Sci Technol 43:3115–3121
41. Doshi H, Ray A, Kothari IL (2007) Biosorption of cadmium by live and dead *Spirulina*: IR spectroscopic, kinetics, and SEM studies. Curr Microbiol 54:213–218
42. Mezaguer M, Kamel N, Lounici H, Kamel Z (2013) Characterization and properties of Pleurotus mutilus fungal biomass as adsorbent of the removal of uranium(VI) from uranium leachate. J Radioanal Nucl Chem 295:393–403
43. Kumar R, Bhatia D, Singh R, Bishnoi NR (2012) Metal tolerance and sequestration of Ni(II), Zn(II) and Cr(VI) ions from simulated and electroplating wastewater in batch process: Kinetics and equilibrium study. Int Biodeter Biodegr 66:82–90
44. Li N, Zeng G, Huang D, Huang C, Lai C, Wei Z, Xu P, Zhang C, Cheng M, Yan M (2015) Response of extracellular carboxylic and thiol ligands (oxalate, thiol compounds) to Pb^{2+} stress in *Phanerochaete chrysosporium*. Environ Sci Pollut R 22:12655–12663
45. Srivastava S, Thakur IS (2006) Biosorption potency of *Aspergillus niger* for removal of chromium(VI). Curr Microbial 53:232–237
46. McLean J, Beveridge TJ (2001) Chromate reduction by a *pseudomonad* isolated from a site contaminated with chromated copper arsenate. Appl Environ Microbiol 67:1076–1084
47. Liu D, Kottke I (2004) Subcellular localization of copper in the root cells of *Allium sativum* by electron energy loss spectroscopy (EELS). Bioresour Technol 94:153–158